

GUEST EDITORS' INTRODUCTION


Special section: Testing inversion algorithms against experimental data

Kamal Belkebir and Marc Saillard

Institut Fresnel, UMR-CNRS 6133, Campus de Saint Jérôme, case 162, 13397 Marseille Cedex 20, France

Published 13 November 2001

Online at stacks.iop.org/IP/17/1565

 This article has associated online supplementary data files

1. Introduction

This special section is devoted to the reconstruction of scattering objects from experimental data. As researchers involved in this topic, we are aware of the importance of testing inversion numerical algorithms against experimental data. Indeed, since inverse scattering problems are ill-posed, their solutions cannot rely upon existence or uniqueness theorems as direct problems do. However, it is often difficult for scientists involved in theoretical and numerical studies to get access to usable experimental data. This is why we think that a database, obtained from laboratory-controlled experiments by people aware of this kind of problem, could be of great interest for the inverse scattering community. The idea is not new; a few years ago, the US Air Force founded experimental works and special sections in *IEEE Transactions on Antennas and Propagation Magazine* [1–4] reported the database as well as the results of the inversion obtained by several teams. These data are known as the Ipswich database. In order to enlarge the scope of applications, and inspired by the Ipswich sessions, we carried out a series of experiments in the anechoic chamber of the Centre Commun de Ressources Micro-ondes (CCRM) at Marseille, France. One of the interesting features of this new database comes from the wide band frequency range considered here, since the max/min frequency ratio is generally equal to 8 for each target. Some contributions benefit from this aspect for their reconstructions, dealing with several frequencies simultaneously or using the frequency hopping technique. The database has also been restricted to homogeneous scatterers, leading some authors to implement algorithms which consider this *a priori* information, via the binary modified gradient method, the binary contrast source inversion method, the controlled evolution of level-sets or a method based on a boundary integral formalism. Another interesting point concerns the modelling of the incident field, which in the database was described by the field recorded on the circle of measurement without a target. Therefore, the value of the incident field in the target area has to be estimated, or optimized along the reconstruction process. Finally, it should be noticed that only two papers deal with the TE polarized data set. This certainly results from the small amount of data available, which does not justify the great amount of work it sometimes implies. Therefore, we have decided to perform new measurements on TE polarization in the near future.

2. Description of the experimental facilities

The experimental setup consists of a large anechoic chamber (figure 1), 14.50 m long, 6.50 m wide and 6.50 m high, with a set of three positioners to adjust antennas or target positions. The frequency range is from 300 MHz to 26.5 GHz. The main applications are:

- radar cross section (RCS) measurements,
- 'spherical' diffraction pattern,
- 'spherical' near-field and far-field antenna measurements.

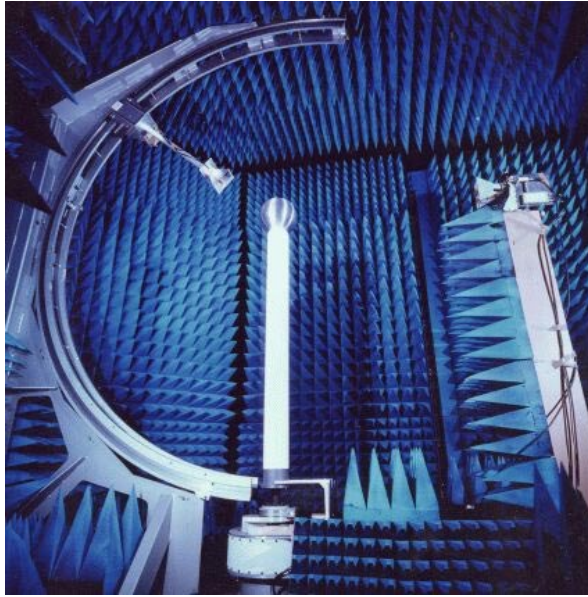


Figure 1. The data are obtained in the anechoic chamber at the Centre Commun de Ressources Micro-ondes (CCRM) at Marseille.

A large variety of experimental configurations can be studied, thanks to four mechanical positioners: they permit us to adjust the orientation of the target and the positions of the antennas placed on the azimuthal arm and on the wagon moving along the vertical circular rail. Both the arm and the rail have a 2 m radius. The fourth positioner, placed at 10.5 m from the target, is devoted to RCS measurements. The antennas are double ridged horn antennas, linearly polarized (ARA DRG 118A, see figure 2). The frequency range of these broad band antennas is from 1 GHz to 18 GHz. Measurements are recorded with the help of a HP8530 network analyser. A PC drives both the analyser and the positioners through an IEEE bus.

3. Two-dimensional configuration

In this work, a 2D bistatic measurement system (as depicted in figure 3) is considered, with an emitter placed at a fixed position on the circular rail, while a receiver is rotating with the arm around a vertical cylindrical target. Two fundamental cases of polarization are investigated,

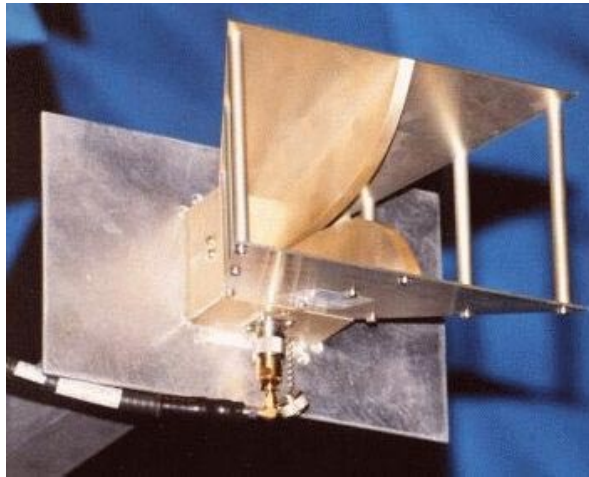


Figure 2. Double ridged horn antennas are used for both emitting and receiving.

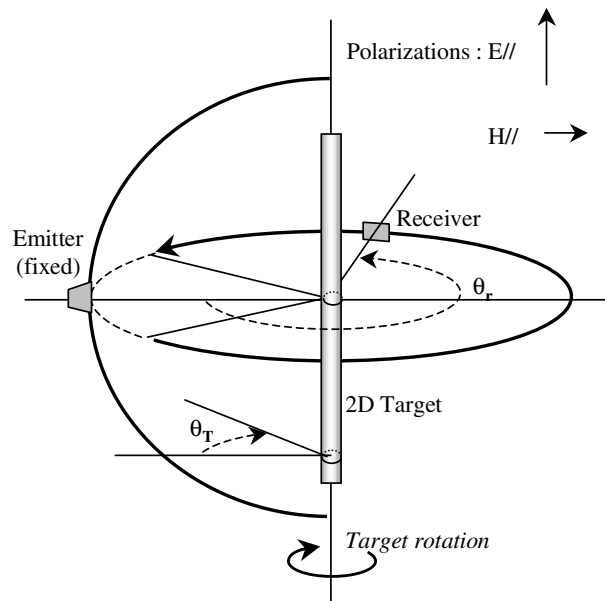


Figure 3. A bistatic measurement system is used to measure the EM field.

denoted by TM and TE, depending on whether the electric or magnetic field is parallel to the cylinder axis, respectively. An example is shown in figure 4.

4. Description of the targets

The following targets (metallic or dielectric) are very large along the vertical direction to present an almost two-dimensional structure. Their cross sections are rectangular, circular or 'U-shaped'.

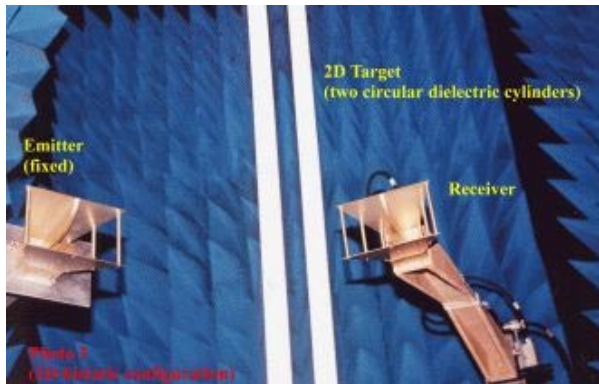


Figure 4. A bistatic measurement system is used to measure the EM field.

4.1. Metallic targets

Two metallic targets (see figure 5) with rectangular and 'U-shaped' cross section are studied. The dimensions of the rectangular cylinder are (25.4×12.7) mm² while those of the 'U-shaped' cylinder are about (80×50) mm².

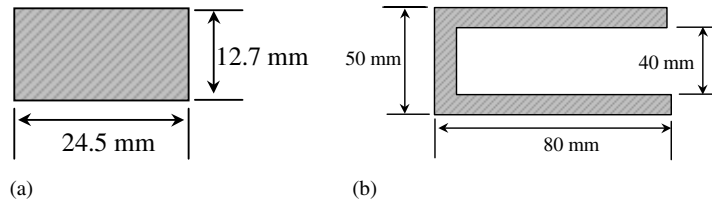


Figure 5. Cross sectional dimensions of the metal targets. (a) Metallic target with a rectangular cross section; (b) metallic target with 'U-shaped' cross section.

4.2. Dielectric targets

The dielectric targets are either composed of one or two filled dielectric cylinders (figure 6), with circular cross section of radius $a = 15$ mm. These cylinders are placed about 30 mm from the azimuthal positioner axis (centre of the experimental setup). The dielectric permittivity has been measured using a waveguide technique [5]. The experimental technique consists of extracting the complex permittivity and permeability from the scattering matrix of the samples. The estimation of the real part of the relative permittivity leads to $\epsilon_r = 3 \pm 0.3$.

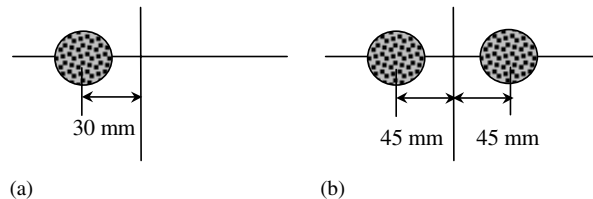


Figure 6. (a) Single circular dielectric cylinder; (b) two-identical circular cylinders.

5. Measurements

The two antennas are placed in the cross sectional plane of the target. For the rectangular target, two cases are considered, according to whether the target is centred or not with respect to the azimuthal positioner axis. Therefore, five target configurations have been dealt with (figure 7).

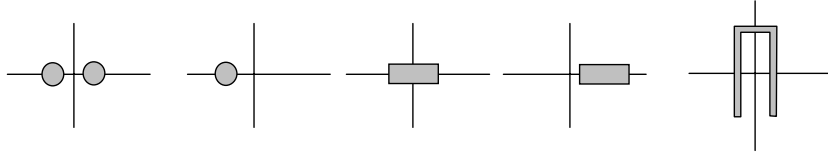


Figure 7. Five configurations of targets have been studied.

Measurements were carried out with the following parameters:

- Distances between:
emitter–centre of the experimental setup : $720 \text{ mm} \pm 3 \text{ mm}$,
receiver–centre of the experimental setup: $760 \text{ mm} \pm 3 \text{ mm}$.
- Angular ranges:
rotation of the target from 0° to 350° in steps of 10° ,
rotation of the receiver from 60° to 300° in steps of 5° .
- Frequency ranges:
from 1 to 8 GHz in steps of 1 GHz, or from 4 to 16 GHz in steps of 4 GHz, or from 2 to 16 GHz in steps of 2 GHz.

Figure 8 presents a comparison between the calculated scattered field and the measured field for the particular case of the centred metallic rectangular cylinder. The computation was achieved thanks to a boundary integral representation of fields [6] assuming that the scatterer is a perfectly conducting cylinder.

6. Layout of the files

All available data (see table 1) are in ASCII files with a 10-line header containing information regarding the target, operating frequencies, polarization, etc. Then follow 7 columns of numbers, which correspond to:

- (a) Integer related to the position of the emitting antenna (source). Number 1 means position $(d_e, 0^\circ)$, number 2 corresponds to the position $(d_e, 10^\circ)$ and so on until 36 $(d_e, 350^\circ)$, where d_e represents the distance between the emitting antenna and the centre of the experimental setup.
- (b) Integer related to the position of the receiving antenna. The numbering is the same as for the emitting antenna but with an angular step of 5° instead of 10° for the emitting antenna.
- (c) Operating frequency in GHz.
- (d) Real part of the total electric field.
- (e) Imaginary part of the total electric field.
- (f) Real part of the incident electric field.
- (g) Imaginary part of the incident electric field.

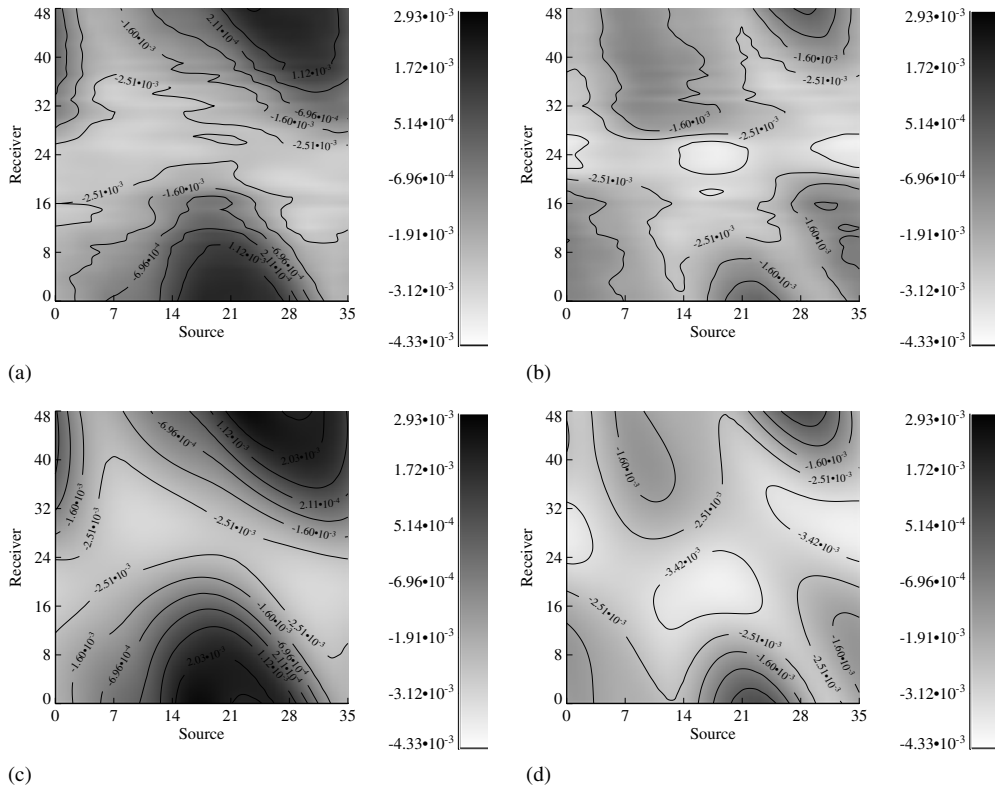


Figure 8. Comparison between the measured and computed scattered field by a metallic cylinder with rectangular cross section (1.27×2.54) cm² at $f = 4$ GHz: (a) and (b) real and imaginary measured scattered field, respectively; (c) and (d) real and imaginary computed scattered field, respectively.

Table 1. Database and related parameters

| Target | File name | Polarization | Frequency (GHz) | |
|--------------------|------------------|--------------|-----------------|----------------|
| | | | Frequency band | Frequency step |
| Single dielectric | dielTM_dec4f.exp | TM | 4–16 | 4 |
| Single dielectric | dielTM_dec8f.exp | TM | 1–8 | 1 |
| Two dielectrics | twodielTM_4f.exp | TM | 4–16 | 4 |
| Two dielectrics | twodielTM_8f.exp | TM | 1–8 | 1 |
| Metallic rectangle | rectTM_cent.exp | TM | 4–16 | 4 |
| Metallic rectangle | rectTM_dece.exp | TM | 2–16 | 2 |
| Metallic rectangle | rectTE_8f.exp | TE | 2–16 | 2 |
| Metallic 'U' | uTM_shaped.exp | TM | 2–16 | 2 |

Notice that all data correspond to electric field measurements. In TM polarization, the measured electric field is parallel to the invariance axis of the cylinder. In TE polarization, only the component orthogonal to both the invariance axis of the cylinder and the direction of illumination is measured. The time dependence is $\exp(i\omega t)$.

Acknowledgments

The authors would like to thank the Editorial Board of *Inverse Problems* for making pages in the journal available for this special section. Particular thanks are due to Ms Elaine Longden-Chapman and Lara Finan for their valuable help in the organization of the session. The authors would also like to thank Dr Pierre Sabouroux for fruitful discussions and for having measured the fields, thus making the data available to the inverse scattering community.

References

- [1] McGahan R V and Kleinman R E 1996 Special session on image reconstruction using real data *IEEE Antennas Propagat. Mag.* **38** (3) 39–59
- [2] McGahan R V and Kleinman R E 1997 Second annual special session on image reconstruction using real data *IEEE Antennas Propagat. Mag.* **39** (2) 7–32
- [3] McGahan R V and Kleinman R E 1999 The third annual special session on image reconstruction using real data, Part 1 *IEEE Antennas Propagat. Mag.* **41** (1) 34–51
- [4] McGahan R V and Kleinman R E 1999 The third annual special session on image reconstruction using real data, Part 2 *IEEE Antennas Propagat. Mag.* **41** (2) 20–40
- [5] Weir W B 1974 Automatic measurement of complex dielectric constant and permeability at microwave frequencies *Proc. IEEE* **62** (1) 33–6
- [6] Saillard M, Vincent P and Maystre D 1996 *A Finite Element Method for Electromagnetic Subsurface Tomography* ed T Itoh, G Pelosi and P Silvester (New York: Wiley) pp 237–65